On the synthesis, structural transformation and magnetocaloric behavior of Ni$_{37.5}$Co$_{12.5}$Mn$_{35}$Ti$_{15}$ melt-spun ribbons

M. López-Cruz, **J. Zamora,** **C. F. Sánchez-Valdés, and** **J. L. Sánchez Llamazares**

On the synthesis, structural transformation and magnetocaloric behavior of Ni$_{37.5}$Co$_{12.5}$Mn$_{35}$Ti$_{15}$ melt-spun ribbons

View Online   Export Citation   CrossMark

M. López-Cruz,[1] J. Zamora,[1] (ID) C. F. Sánchez-Valdés,[2] (ID) and J. L. Sánchez Llamazares[1,a] (ID)

AFFILIATIONS

[1] Instituto Potosino de Investigación Científica y Tecnológica A.C., Camino a la Presa San José 2055, Col. Lomas 4ª Sección, San Luis Potosí S.L.P. 78216, Mexico

[2] Departamento de Física y Matemáticas, División Multidisciplinaria en Ciudad Universitaria, Instituto de Ingeniería y Tecnología, Universidad Autónoma de Ciudad Juárez (UACJ), Ciudad Juárez, 32310 Chihuahua, Mexico

Note: This paper was presented at the 65th Annual Conference on Magnetism and Magnetic Materials.
[a] Author to whom correspondence should be addressed: jose.sanchez@ipicyt.edu.mx

ABSTRACT

We fabricated Ni$_{37.5}$Co$_{12.5}$Mn$_{35}$Ti$_{15}$ melt-spun ribbons at linear wheel speeds (WS) of 20 and 8 ms^{-1} (series A and B, respectively). The effect of a short time thermal annealing (30 min.) between 1023 K and 1173 K on the martensitic-like structural transition and the crystal structure, microstructure and magnetic entropy change $\Delta S_M(T)$ curves and related parameters for as-solidified (AS) samples of series A were studied. Whereas the Curie temperature of austenite (AST) T_C^A keeps nearly constant, both the reduction of the solidification rate and the increase on the thermal annealing temperature increase the temperature of the structural transformation reducing the magnetization change across the AST to martensite (MST) transition. The martensitic transformation (MT) in AS samples undergoes from a B2-type ferromagnetic (FM) AST with T_C^A = 328 K to a monoclinic martensite (MST); SEM images evidenced a partially grain-oriented microstructure formed by columnar in shape-elongated grains with their major axis oriented along the thermal gradient during solidification. Magneto-structural transition for AS ribbons of series A occurs in the vicinity of room temperature and is accompanied by a magnetization change of around 63 Am^{2}kg^{-1}. For a magnetic field change of 2 T these samples showed a maximum magnetic entropy change $|\Delta S_M|^{max}$ of 13.8 (9.5) J kg^{-1} K^{-1} for the MST→AST (AST→MST) transformation. This is below the previously reported for this alloy composition (27.2 J kg^{-1} K^{-1}), and is related to the broader magneto-structural transition.

I. INTRODUCTION

The sizeable magnetocaloric,[1–4] elastocaloric,[5] barocaloric[6] and magneto-strain[7] effects around temperature (RT) associated to the martensitic transformation (MT) found in the newly reported all-3d-metal quaternary Ni-Mn-Co-Ti alloys are a strong motivation for their further investigation. These alloys also show excellent mechanical properties,[1,3,4] which contrast with the widely studied (Ni-Mn-X)-based Heusler alloys (X = Ga, In, Sn and Sb) that are quite brittle. The realization of martensitic-like magnetostructural transformation was first reported by Wei et al. in bulk Ni$_{50-x}$Co$_x$Mn$_{35}$Ti$_{15}$ (x = 8, 9.5),[1] and Mn$_{50}$Ni$_{40-x}$Co$_x$Ti$_{10}$ (x = 8.0, 9.5) alloys,[7] who also pointed out most of the physical phenomena that gave rise to the

above-mentioned functionalities. The MT takes place from a high-temperature ferromagnetic (FM) austenite (AST) with the cubic B2-type crystal structure to a weak magnetic martensite with a monoclinic crystal structure ($P2/m$).[1–4,7] With the increase in the Co content, the Curie temperature of AST T_C^A increases, whereas the temperature of the structural transition can be tuned in a wide temperature interval from above to well below room temperature (RT).[1,4] From the available literature it seems that the temperature of the MT is strongly influenced by microstructural features.[1,3] In most of the early experimental reports, these alloys, both in bulk or as melt-spun ribbons, showed a broad magnetostructural transition.[1,3] However, in a more recent study Neves Bez et al. produced rapidly solidified Ni$_{50-x}$Co$_x$Mn$_{35}$Ti$_{15}$ melt-spun ribbons (12 ≤ x ≤ 15),

with a high chemical homogeneity and a quite abrupt magneto-structural transition.[4] For the quaternary alloy $Ni_{37.5}Co_{12.5}Mn_{35}Ti_{15}$ they obtained one of the highest maximum magnetic entropy change $|\Delta S_M|^{max}$ values around RT ever found for a first-order magnetocaloric material for a magnetic field change $\mu_o \Delta H$ of 2 T. Considering the noticeable current interest in these multifunctional alloys, we selected the $Ni_{37.5}Co_{12.5}Mn_{35}Ti_{15}$ alloy and produced melt-spun ribbons at two surface linear speeds of the rotating copper wheel, 8 ms^{-1} and 20 ms^{-1} (the latter was the same WS used in Ref. [4]). Finally, several aspects of interest, such as the influence of a 30 minutes thermal annealing at temperatures between 1023 K and 1173 K on the MT as well as the magnetic entropy change for (AS) samples produced at 20 ms^{-1}, were studied.

II. EXPERIMENTAL PROCEDURE

Two 4 grams arc-melted ingots of nominal composition $Ni_{37.5}Co_{12.5}Mn_{35}Ti_{15}$ were fabricated from pure elements ($\geq$ 99.9 %). The samples were flipped and re-melted several times to improve their starting chemical homogeneity; the mass of the samples remained unchanged. Then, the Edmund Buhler model SC melt spinner system was used to produce ribbon flakes under UAP Ar at linear speeds of the copper wheel of 20 ms^{-1} and 8 ms^{-1} (hereafter referred as series A and B, respectively); the rest of process parameters were the same for both series. Some ribbon samples were thermally annealed in vacuumed sealed quartz ampoules at 1023 K, 1073 K, 1123 K, and 1173 K for 30 minutes; annealing ended by quenching in iced water. The phase constitution for as-solidified ribbons was qualitatively determined from X-ray powder diffraction (XRD) patterns collected in a Rigaku Smartlab diffractometer (CuK$_{\alpha 1}$). Microstructural and semi-quantitative elemental chemical composition analyses were performed in a FEI QUANTA 200 SEM equipped with an EDS system. Differential scanning calorimetry (DSC) analyses were done with a temperature sweep rate of 10 Kmin^{-1} in a model Q200 system from TA Instruments. The initial and final temperatures of the direct and reverse MT (M_S and M_f, and A_S and A_f, respectively), were determined by a simple extrapolation, whereas the thermal hysteresis ΔT_{hyst} was estimated

as $\Delta T_{hyst} = A_f - M_S$. Magnetization measurements were done in a 9 T QD PPMS® Dynacool® system using the VSM option; the magnetic field was applied along ribbon length to reduce the internal demagnetizing field. Finally, the thermal dependencies of the magnetization were measured with a temperature sweep rate of 1.0 Kmin^{-1} following zero-field-cooling (ZFC) and field-cooling (FC) regimens under static magnetic fields of 5 mT and 2 T [referred as $M(T)^{5mT}$ and $M(T)^{2T}$, respectively].

III. RESULTS AND DISCUSSION

Figs. 1(a) and (b) show the typical microstructure at the cross section of as-solidified ribbon samples for both series. The main difference between them lies in the average ribbon thickness $\langle d \rangle$ that, as expected,[8] is higher in samples produced at a higher solidification rate (measured $\langle d \rangle$ values were ~ 42-48 µm and ~ 80-85 µm, for series A and B, respectively). The microstructure of both batches is formed by columnar in shape grains whose longer axis tends to align across the ribbon thickness. This denotes a strong effect of the thermal gradient during solidification on crystal growth that gives rise to partial texture. These microstructural features are similar to those reported by other authors.[2,3] Considering the different scales of the pictures, the width of columnar grains is higher for series B (~ 3.5-4.0 µm versus ~ 2.0-2.5 µm, respectively). EDS spectra, shown in Figs. S1(a) and (b) (supplementary material), only display the peaks coming from the four constituents (with the exception of those of C and Al peaks that come from the sample holder and ribbon used to attach samples). For both samples, the intensity of the peaks is similar suggesting that, within uncertainty of the determination (~ 1.0 at. %), their average elemental chemical composition is quite close: $Ni_{36.3}Co_{12.6}Mn_{36.2}Ti_{14.9}$ (series A) and $Ni_{37.1}Co_{12.4}Mn_{36.2}Ti_{14.3}$ (series B). They are also close to the nominal one. The results correspond to nearly 20 EDS analyses carried out on both ribbon surfaces and the cross-section.

The XRD patterns for as-solidified ribbons samples of series A and B appear in Figs. 1(c) and (d). In both cases the phase constitution agrees with the ones expected from the cooling pathway of the DSC scans depicted at the inset of Fig. 1(c). In consonance with
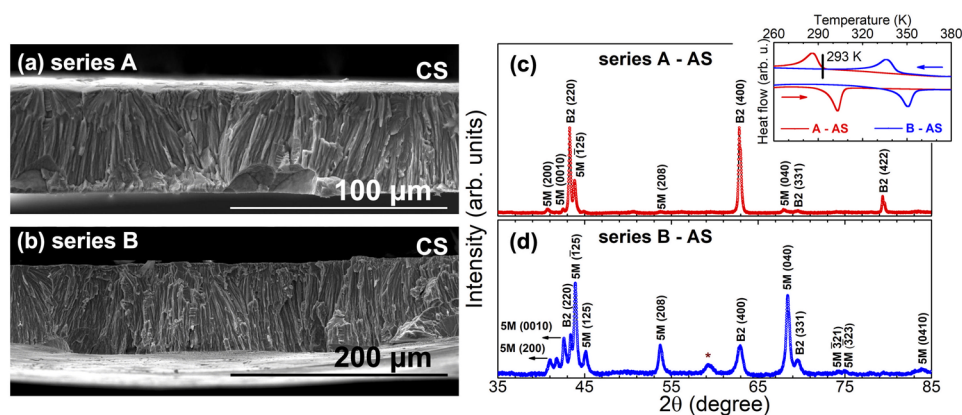
FIG. 1. SEM micrograph of the typical microstructure at the cross-section XRD pattern of as-solidified $Ni_{37.5}Co_{12.5}Mn_{35}Ti_{15}$ melt-spun ribbons of series A [(a) and (c)] and B [(b) and (d)], respectively. Inset in (c): DSC curves for both samples. The vertical line drawn in the graph indicates the approximate temperature at which the XRD patterns were collected.
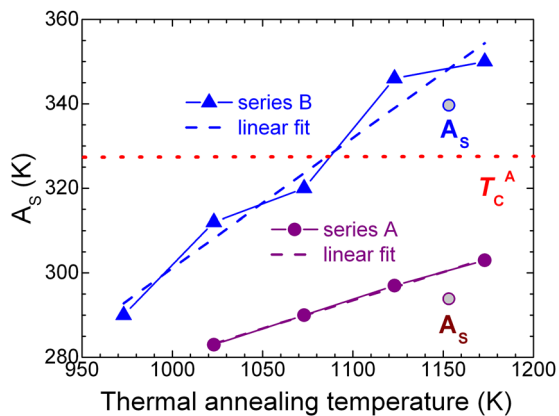
FIG. 2. A_S as a function of the thermal annealing temperature of both series of samples (the horizontal dashed line indicates T_C^A).

earlier reports,[1–4] the major phases indexed in the patterns were a cubic B2-type AST (series A; a_{B2} = 5.906 Å) and a five-layer modulated (5M) monoclinic MST (series B; a_{B2} = 5.895 Å, a_{5M} = 4.400 Å, b_{5M} = 5.480 Å, c_{5M} = 21.216 Å, and β = 92.48°), respectively. Due to the vicinity of RT to A_S the higher intensity XRD peaks of MST appear as a minor reflection in the pattern of Fig. 1(d). As in previous studies,[2,3] the XRD pattern for MST shows a minor unidentified peak at 2θ = 59.3° (indicated by an asterisk), that was not observed for this alloy in Ref. 4.

The DSC scans of thermally annealed samples of both series are shown in Figs. S2(a) and (b). As Fig. 2 shows A_S increases almost linearly upon the increase of the thermal annealing temperature (with

a different slope for each series). However, notice that in the AS samples of both series A_S was found outside of the linear dependence. The characteristic temperatures of the direct and reverse MT transitions and ΔT_{hyst} of the transformation are summarized in Table S1.

In order to highlight some of the distinctive characteristics of the magnetostructural transition in the studied ribbon samples, Fig. 3 compares the $M(T)^{5mT}$ and $M(T)^{2T}$ for selected samples of both series. In Fig. 3(a) the $M(T)^{5mT}$ and DSC curves for AS samples of series A and B are presented. With the reduction of the wheel linear speed (and thus the solidification rate), the structural MT markedly increases around 48 K, whereas in oth series the T_C^A [determined from the minimum of the $dM/dT(T)$ curve at 5 mT] keeps around 328 K. In fact, it must be noticed that for series B A_S exceeds T_C^A. Hence, as Figs. 3(a) and (b) show the magnetic transition for ribbon samples of series B is negligible at 5 mT, while at 2 T is broad and accompanied by a low magnetization change ΔM. In contrast, for series A the estimated magnetization change at 2 T was $\Delta M^{2T} \sim 63$ Am^{2}kg^{-1}. For these reasons, the magnetocaloric characterization presented below has been only focused on this sample. For AS Mn$_{50}$Ni$_{31.5}$Co$_{8.5}$Ti$_{10}$ alloy ribbons Ma et al. reported a moderate increase in the MT temperature of about 14 K when the WS is reduced from 25 ms^{-1} to 15 ms^{-1},[9] a fact that has been correlated with an increase of the crystal defects density with the decrease in the average grain size, and has been observed in other Heusler alloys.[10,11] If the ZFC-FC $M(T)^{5mT}$ curves for AS ribbons of series A are roughly compared with those measured by Neves Bez et al. under 0.1 T,[4] is noticed that for our samples T_C^A is ~ 6 K lower, whereas the temperature of the MST→AST (AST→MST) transition is higher in ~ 16 K. Considering that T_C^A is mainly determined by the alloy composition,[1] this difference has been attributed to slight
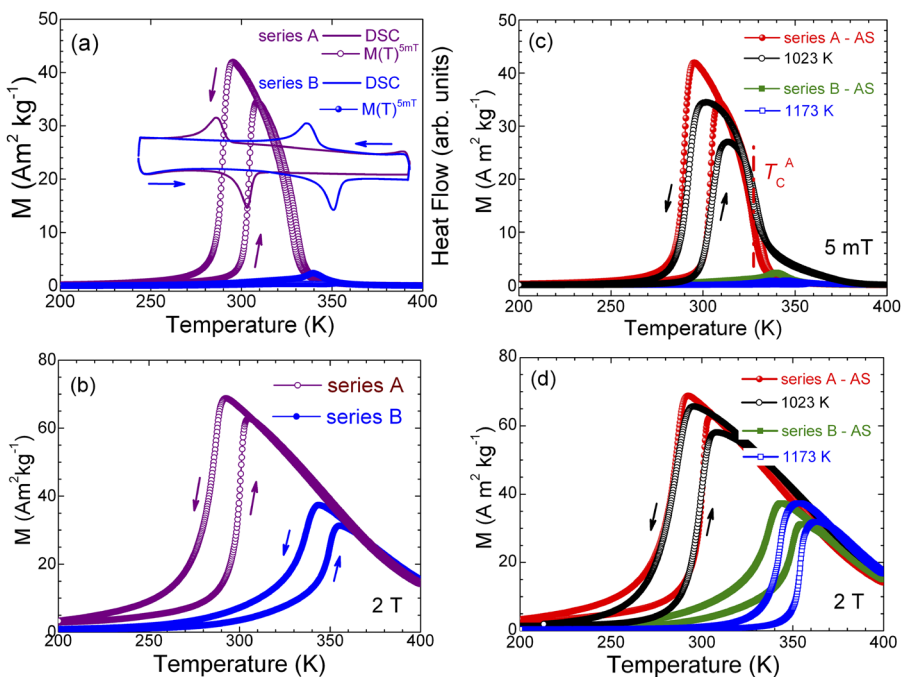

FIG. 3. DSC and $M(T)$ curves at 5 mT (a) and $M(T)$ at 2 T (b) of as-solidified melt-spun ribbon sample of series A and B. Comparison of the $M(T)$ curves at 5 mT (c) and 2 T (d) of as-solidified and thermally annealed samples of series A and B.

differences in the final chemical composition between our samples and those produced in Ref. 4 where the authors only referred to the nominal composition. The difference in the structural transition temperature is comprehensible due to being strongly influenced by the solidification rate and, of course, the selected melt spinning process variables which also depend on the technical features of the melt spinning apparatus used. The effect of thermal annealing on the magnetostructural transition has been illustrated in Figs. 3(c) and (d) in which $M(T)^{5mT}$ and $M(T)^{2T}$ for AS and annealed samples have been compared. For comparison, we selected annealed samples that had a similar A_S temperature, determined from the $M(T)^{5mT}$ curve, than the as-solidified ones that in this case correspond to annealed ribbons at 1023 K and 1173 K for series A and B, respectively. The graphs show, that after the thermal annealing neither the total magnetization change at 2 T nor the abruptness of the magnetostructural transition or the T_C^A had significantly changed, (but it is highlighted that this result is restricted to the annealing temperatures tested in the present work, i.e., from 1023 K to 1173 K). Ref. 3 similarly demonstrated that a short thermal annealing (10 min.) between 923 and 1123 K had a marginal effect on the modification of the magnetostructural transition and the related $|\Delta S_M|^{max}$. It is known that the optimization of the magnetostructural transition towards the enhancement of magnetocaloric properties (namely $|\Delta S_M|^{max}$ and $|\Delta T_{ad}|^{max}$) in (Ni-M)-based Heusler alloys is closely connected with to a proper selection of the annealing temperature with respect to the alloy melting point (in our case the melting point of the processed alloys was roughly estimated as ~ 1400 K from the reading of an infrared radiation pyrometer, model KT 18.03RLL from Heitronics, used in the melt spinner system).[12] Hence, our results suggest that the higher thermal treatment temperature used in the present study was not high enough to activate neither the diffusion nor atomic rearrangement processes that optimize the chemical homogeneity and crystallographic ordering.

The insets in Figs. S3(a) and (b) display the sets $M(\mu_o H)$ curves measured up to 2 T in the temperature range of the inverse and direct magnetostructural transitions, respectively, for AS samples of series A. The $\Delta S_M(T)$ curves were determined from them by the numerical integration of the Maxwell relation. Due to the first-order nature of the transition, the thermal protocol called Ref. 13 as *back-and-forward* was followed to measure each $M(\mu_o H)$ curve, this is: for the MST-to-AST (AST-to-MST) transition $\mu_o H$ was set to zero and the sample was heated to 400 K (cooled to 200 K), cooled to 200 K (heated to 400 K), and then slowly heated (cooled) in No Overshoot mode to reach the measuring temperature. Figs. S3(a) and (b) show the computed Arrott plots for both transitions that, according to the Banerjee criterion,[14] underline their first-order nature. Fig 4 compares the $|\Delta S_M(T)|$ curves for different $\mu_o \Delta H$ values determined for both transitions with those reported in Ref. 4 for the MST→AST transition. The produced ribbons show a broader $\Delta S_M(T)$ curve for the reverse transition with a peak value $|\Delta S_M|^{max}$ reduced around a 50 %: 13.8 $Jkg^{-1}K^{-1}$ versus 27.2 $J kg^{-1}K^{-1}$. The latter is related to the broader transition since $|\Delta S_M|$ is proportional to $|dM/dT|$, a fact that is indirectly quantified by the full-width at half-maximum of the $\Delta S_M(T)$ curves (δT_{FWHM}); for $\mu_o \Delta H$ = 2 T, δT_{FWHM}, was estimated as 7 K versus ~ 3 K for the compared curve. This suggests that in these alloys the width of the transition strongly depends on the processing conditions. However, comparable $|\Delta S_M|^{max}$ values have
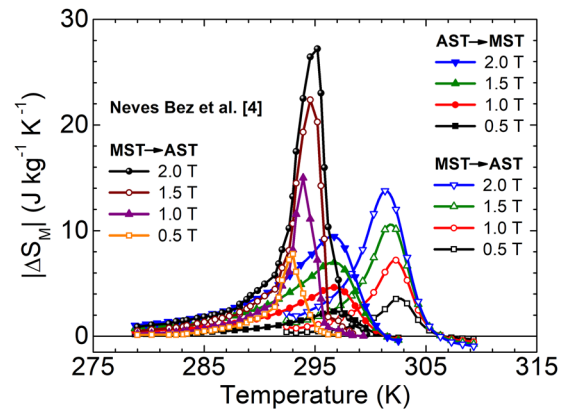
FIG. 4. $|\Delta S_M(T)|$ curves obtained for both transitions for as-solidified melt-spun ribbon sample of series A compared with those reported by Neves Bez *et al.* for the MST→AST transition (0.5 T ≤ $\mu_o \Delta H$ ≤ 2 T).[4]

been reported by other authors for alloys with a similar composition: $Ni_{35}Co_{15}Mn_{35}Ti_{15}$ (~ 10 $Jkg^{-1}K^{-1}$; bulk),[1] $Ni_{36}Co_{14}Mn_{35.7}Ti_{14.3}$ (~ 10 $Jkg^{-1}K^{-1}$; AS ribbons),[2] and $Ni_{36.5}Co_{13.5}Mn_{35}Ti_{15}$ (~11 $Jkg^{-1}K^{-1}$; ribbons annealed at 1123 K for 10 min.).[3] Table S2 summarizes the significant magnetocaloric properties through both transitions including the refrigerant capacity (RC) values, that were calculated as: (i) RC-1 = $|\Delta S_M|^{max}$ × δT_{FWHM}, where δT_{FWHM} = T_{hot} - T_{cold}; (ii) by calculating the area under the $\Delta S_M(T)$ curve between T_{hot} and T_{cold} (RC-2); and (iii) by maximizing the product ΔS_M × δT below the $\Delta S_M(T)$ curve (RC-3; Wood and Potter criterion).[15]

IV. CONCLUSION

From the present study, in which melt-spun ribbons of the all-3-d-metal Heusler alloy $Ni_{37.5}Co_{12.5}Mn_{35}Ti_{15}$ were produced at two different wheel speeds (20 ms^{-1} and 8 ms^{-1}), it was concluded that: (a) the structural transition temperature strongly depends on the solidification rate. In the produced ribbon samples, the MT increased ~ 48 K with the reduction of the linear wheel speed from 20 to 8 ms^{-1}. Hence, as the T_C^A is basically determined by the chemical composition of the alloy, the solidification rate is a relevant parameter that should be carefully controlled in order to get the magnetostructural transition at a desired temperature with the largest possible $|\Delta S_M|^{max}$ value; (b) the temperature of the structural MT increased with the increment of the thermal annealing temperature. However, neither the total magnetization change nor the abruptness of the magnetostructural transition or T_C^A significantly changed with the thermal treatments performed. Therefore, a crucial aspect towards the optimization of the magnetocaloric properties of ribbon samples in the as-solidified state demands a deeper understanding of the effect of the others synthesis parameters involved in the melt spinning process as well as the test of higher annealing temperatures; (c) in comparison with the previous data reported in the literature, the inferior $|\Delta S_M|^{max}$ values obtained in the produced as-solidified ribbon samples of series A were mainly related to attainment of a broader magnetostructural transition.

SUPPLEMENTARY MATERIAL

See supplementary material for: (a) the characteristic EDS spectra of melt-spun ribbon samples of both series (Fig. S1); (b) the DSC curves of as-solidified and thermally annealed ribbon samples of both series (Fig. S2); (c) a Table containing the starting and finishing temperatures for the MST-AST and AST-MST transitions of as-solidified and thermally annealed ribbon samples of both series determined from DSC (Table S1); (d) the Arrott plots and sets of isothermal magnetization curves measured across the inverse and direct martensitic transition for as-solidified ribbon samples of series A (Fig. S3), and; (e) a Table containing $|\Delta S_M|^{max}$, estimated refrigerant capacity and related temperature parameters under $\mu_o \Delta H = 1$ and $2\,T$ of as-solidified melt-spun ribbons of series A (Table S2).

ACKNOWLEDGMENTS

DATA AVAILABILITY

The data that support the findings of this study are available within the article and its supplementary material.

REFERENCES

[1] Z. Y. Wei, E. K. Liu, J. H. Chen, Y. Li, G. D. Liu, H. Z. Luo, X. K. Xi, H. W. Zhang, W. H. Wang, and G. H. Wu, "Realization of multifunctional shape-memory ferromagnets in all-d-metal Heusler phases," Appl. Phys. Lett. **107**, 022406 (2015).

[2] K. Liu, X. Han, K. Yu, C. Ma, Z. Zhang, Y. Song, S. Ma, H. Zeng, C. Chen, X. Luo, S. U. Rehman, and Z. Zhong, "Magnetic-field-induced metamagnetic reverse martensitic transformation and magnetocaloric effect in all-d-metal Ni$_{36.0}$Co$_{14.0}$Mn$_{35.7}$Ti$_{14.3}$ alloy ribbons," Intermetallics **110**, 106472 (2019).

[3] K. Liu, S. Ma, C. Ma, X. Han, K. Yu, S. Yang, Z. Zhang, Y. Song, X. Luo, C. Chen, S. U. Rehman, and Z. Zhong, "Martensitic transformation and giant magneto-functional properties in all-d-metal Ni-Co-Mn-Ti alloy ribbons," J. Alloys Compd. **790**, 78 (2019).

[4] H. Neves Bez, A. K. Pathak, A. Biswas, N. Zarkevich, V. Balema, Y. Mudryk, D. D. Johnson, and V. K. Pecharsky, "Giant enhancement of the magnetocaloric response in Ni-Co-Mn-Ti by rapid solidification," Acta Mater. **173**, 225 (2019).

[5] Z. Y. Wei, W. Sun, Q. Shen, Y. Shen, Y. F. Zhang, E. K. Liu, and J. Liu, "Elastocaloric effect of all-d-metal Heusler NiMnTi(Co) magnetic shape memory alloys by digital image correlation and infrared thermography," Appl. Phys. Lett. **114**, 101903 (2019).

[6] Z. Wei, Y. Shen, Z. Zhang, J. Guo, B. Li, E. Liu, Z. Zhang, and J. Liu, "Low-pressure-induced giant barocaloric effect in an all-d-metal Heusler Ni$_{35.5}$Co$_{14.5}$Mn$_{35}$Ti$_{15}$ magnetic shape memory alloy," APL Mater. **8**, 051101 (2020).

[7] Z. Y. Wei, E. K. Liu, Y. Li, X. L. Han, Z. W. Du, H. Z. Luo, G. D. Liu, X. K. Xi, H. W. Zhang, W. H. Wang, and G. H. Wu, "Magnetostructural martensitic transformations with large volume changes and magneto-strains in all-d-metal Heusler alloys," Appl. Phys. Lett. **109**, 071904 (2016).

[8] R. C. Budhani, T. C. Goel, and K. L. Chopra, "Melt-spinning technique for preparation of metallic glasses," Mater. Sci. **4**, 549–561 (1982).

[9] C. Ma, K. Liu, X. Han, S. Yang, N. Ye, and J. Tang, "Martensitic transformation and magnetocaloric effect in melt-spun Mn$_{50}$Ni$_{31.5}$Co$_{8.5}$Ti$_{10}$ all-3d-metal alloy ribbons," J. Magn. Magn. Mater. **493**, 165733 (2020).

[10] A. Quintana-Nedelcos, J. L. Sánchez Llamazares, D. Ríos-Jara, A. G. Lara-Rodríguez, and T. García-Fernández, "Effect of quenching rate on the average grain size and martensitic transformation temperature in rapidly solidified polycrystalline Ni$_{50}$Mn$_{37}$In$_{13}$ alloy ribbons," Phys. Status Solidi A **210**, 2159–2165 (2013).

[11] C. O. Aguilar-Ortiz, J. P. Camarillo-García, J. Vergara, P. Álvarez-Alonso, D. Salazar, V. A. Chernenko, and H. Flores-Zúñiga, "Effect of solidification rate on martensitic transformation behavior and adiabatic magnetocaloric effect of Ni$_{50}$Mn$_{35}$In$_{15}$ ribbons," J. Alloys Compd. **748**, 464 (2018).

[12] A. Taubel, T. Gottschall, M. Fries, S. Riegg, C. Soon, K. P. Skokov, and O. Gutfleisch, "A comparative study on the magnetocaloric properties of Ni-Mn-X(-Co) Heusler alloys," Phys. Status Sol. B **255**, 1700331 (2018).

[13] A. Quintana-Nedelcos, J. L. Sánchez Llamazares, C. F. Sánchez-Valdés, P. Álvarez Alonso, P. Gorria, P. Shamba, and N. A. Morley, "On the correct estimation of the magnetic entropy change across the magneto-structural transition from the Maxwell relation: Study of MnCoGeB$_x$ alloy ribbons," J. Alloys Compd. **694**, 1189–1195 (2017).

[14] S. K. Banerjee, "On a generalized approach to first and second order magnetic transitions," Phys. Lett. **12**, 16–17 (1964).

[15] P. Gorria, J. L. Sánchez Llamazares, P. Álvarez, M. J. Pérez, J. Sánchez Marcos, and J. A. Blanco, "Relative cooling power enhancement in magneto-caloric nanostructured Pr$_2$Fe$_{17}$," J. Phys. D: Appl. Phys. **41**, 192003 (2008).

SUPPLEMENTARY MATERIAL

On the synthesis, structural transformation and magnetocaloric behavior of Ni$_{37.5}$Co$_{12.5}$Mn$_{35}$Ti$_{15}$ melt-spun ribbons

M. López-Cruz,[1] J. Zamora,[1] C.F. Sánchez-Valdés,[2] and
J.L. Sánchez Llamazares[1, a]

[1] Instituto Potosino de Investigación Científica y Tecnológica A.C., Camino a la Presa San José 2055, Col. Lomas 4ª sección, San Luis Potosí, S.L.P. 78216, México
[2] Departamento de Física y Matemáticas, División Multidisciplinaria en Ciudad Universitaria, Instituto de Ingeniería y Tecnología, Universidad Autónoma de Ciudad Juárez (UACJ), Ciudad Juárez, 32310 Chihuahua, México.

[a] Corresponding author: jose.sanchez@ipicyt.edu.mx
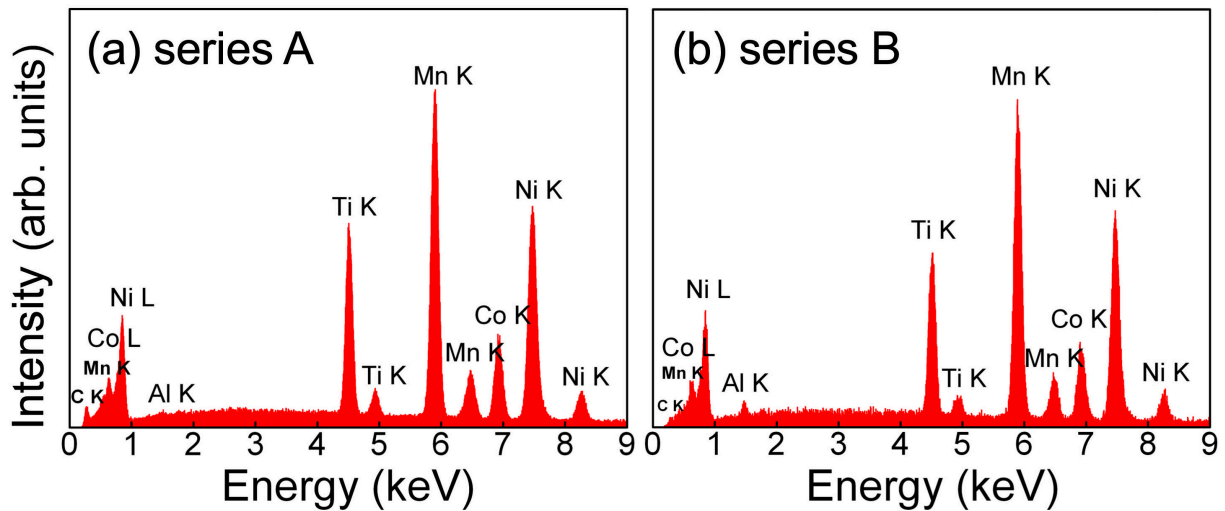
FIG. S1. EDS spectrum of as-solidified Ni$_{37.5}$Co$_{12.5}$Mn$_{35}$Ti$_{15}$ melt-spun ribbons of series A (a) and B (b), respectively.
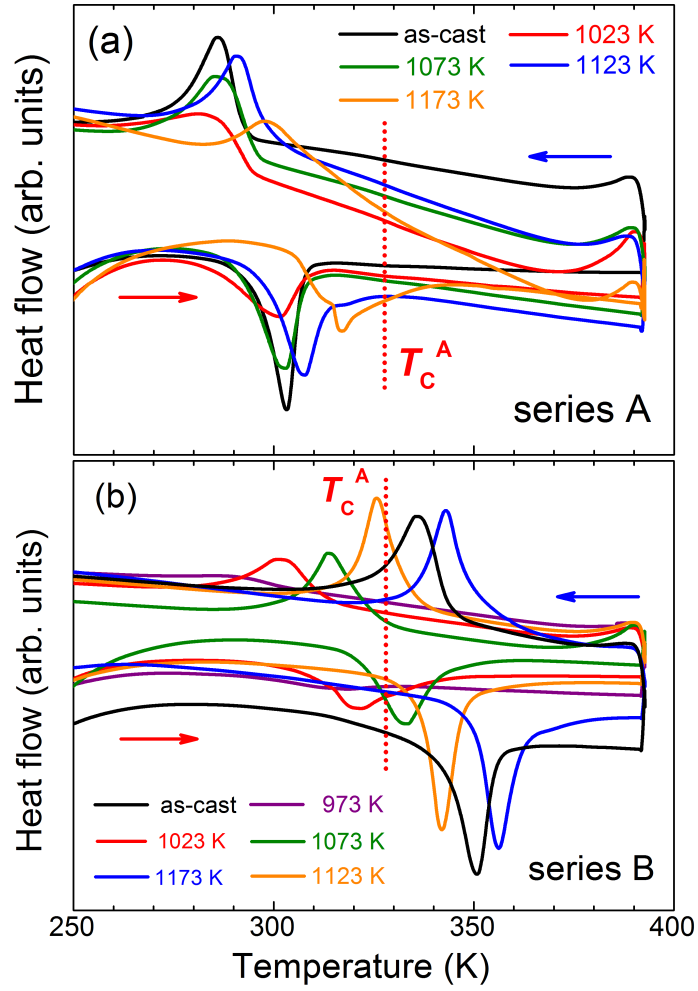
FIG. S2. DSC curves of as-solidified and thermally annealed ribbon samples of series A (a) and B (b). The vertical dashed lines in both figures indicate the Curie temperature T_C^A of the austenite phase (that was determined from the first derivative of the $M(T)^{5mT}$ curves).

TABLE S1. Starting and finishing temperatures for the MST→AST and AST→MST transitions of as-solidified and thermally annealed ribbon samples of series A and B determined from DSC.

heat treatment	Series A					Series B				
	A_S (K)	A_f (K)	M_S (K)	M_f (K)	ΔT_{hyst} (K)	A_S (K)	A_f (K)	M_S (K)	M_f (K)	ΔT_{hyst} (K)
as-solidified	294	308	293	276	15	341	356	344	325	12
973 K	-	-	-	-	-	290	328	300	277	28
1023 K	283	310	296	273	14	312	330	311	288	19
1073 K	290	309	296	273	13	320	344	327	303	17
1123 K	297	316	299	280	17	346	349	335	318	14
1173 K	303	340	-	286	-	350	363	352	335	11
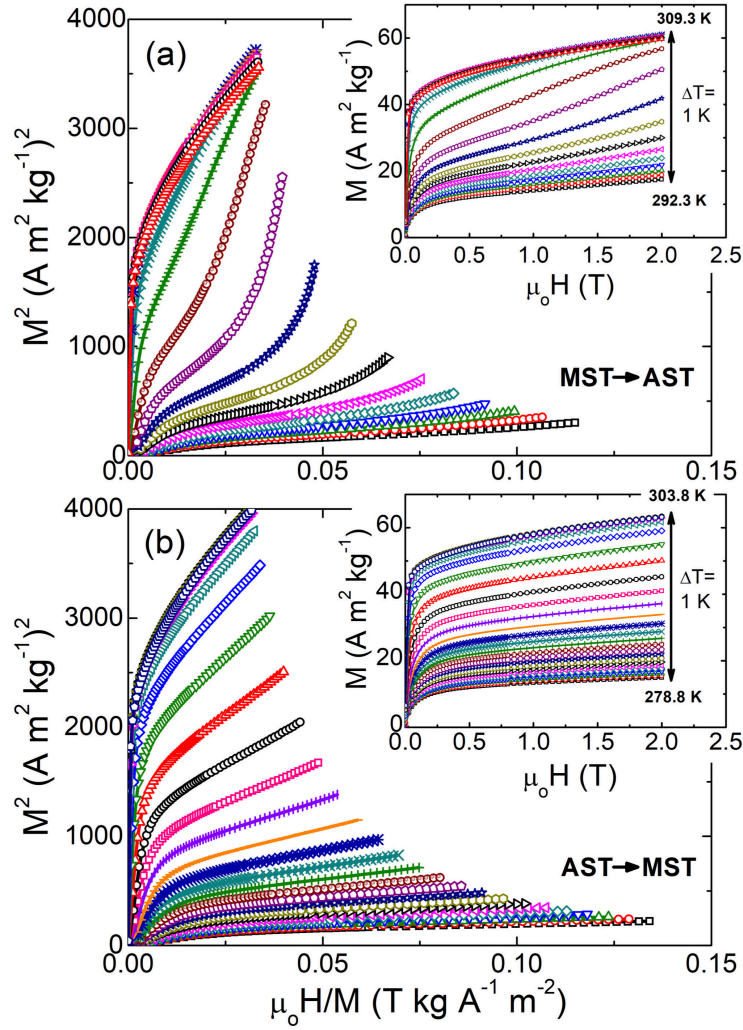
FIG. S3. Arrott plots (i.e., M^2 vs. $\mu_o H/M$) and sets of isothermal magnetization $M(\mu_o H)$ curves (shown at the inset of the respective graphs) measured across the inverse (a) and direct (b) martensitic transition for as-solidified ribbon samples of series A.

TABLE S2. $|\Delta S_M|^{max}$, estimated refrigerant capacity and related temperature parameters under $\mu_o \Delta H = 1$ and 2 T of as-solidified $Ni_{37.5}Co_{12.5}Mn_{35}Ti_{15}$ melt-spun ribbons of series A.

	Transition	MST→AST		AST→MST	
	$\mu_o \Delta H$	1 T	2 T	1 T	2 T
$\mathbf{\|\Delta S_M\|}$ ^{max} (Jkg^{-1}K^{-1})		7.2	13.8	4.6	9.5
RC-1 (Jkg^{-1})		29	64	33	70
RC-2 (Jkg^{-1})		22	51	26	55
δT_{FWHM} (K)		4	4	7	7
T_{hot} (K)		304	303	299	299
T_{cold} (K)		300	299	292	292
RC-3 (Jkg^{-1})		14	33	16	35
$\delta T^{RC\text{-}3}$ (K)		4	4	7	8
$T_{hot}^{RC\text{-}3}$ **(K)**		304	303	299	299
$T_{cold}^{RC\text{-}3}$ **(K)**		300	299	292	291

3